Comparison between axionlike and power law potentials in a cosmological background

Md. Wali Hossain[*] and Afaq Maqsood[†]
Department of Physics, Jamia Millia Islamia, New Delhi, 110025, India

(Received 30 November 2023; accepted 18 April 2024; published 9 May 2024)

In this paper, we compare the scalar field dynamics in the axionlike and power law potentials for both positive and negative values of the exponents. We find that, for positive exponents, both potentials exhibit similar scalar field dynamics, and it can be difficult to distinguish them at least at the background level. Even though the potentials are oscillatory in nature, for positive exponents scaling solutions can be achieved for larger values of the exponent for which the dynamics can be different during early times. Because of the presence of this scaling nature, there is a turnaround in the values of the scalar field equation of state as we increase the values of the exponent in both potentials. This indicates the deviation from the oscillatory behavior for the larger values of the exponent. For negative values of the exponent, the dynamics of the scalar field is distinguishable, and axionlike potential can give rise to cosmologically viable tracker solutions unlike the power law potentials. For negative values of the exponent, the axionlike potential can behave like a cosmological constant around its minima, and the dark energy scale can be related to the potential scale. Because of the cosmological-constant-like behavior of the axionlike potential for negative exponent around its minima, the late time dynamics can be similar to Lambda cold dark matter (ΛCDM), and we get a similar observational constraint on the parameters for both ΛCDM and the axionlike potential with a negative exponent. So, while for positive exponents we may not distinguish the two potentials, for negative exponents the dynamics of the scalar field is distinguishable.

DOI: 10.1103/PhysRevD.109.103512

I. INTRODUCTION

Recent cosmological observations suggest that our present Universe is expanding with an acceleration [1–4]. The reason for the late time acceleration still remains a mystery, but the cosmological constant (CC) Λ has appeared as the simplest yet most viable explanation, especially by the observations of the cosmic microwave background (CMB) radiation [3,5]. However, the CC is plagued with two issues, namely, the fine-tuning problem [6] and the cosmic coincidence problem [7,8]. This motivates us to look for other possible solutions, e.g., make dark energy dynamical [9,10] or modify gravity [11]. In this paper, we study the former case. Considering a scalar field instead of the CC makes the equation of state (EOS) dynamical. We study the cosmological dynamics of the scalar field for two specific potentials: the axionlike [12–15] and power law potentials [16].

Slowly rolling scalar fields known as the quintessence field [16–18] can also explain the late time acceleration [9]. Scalar fields can also solve the cosmic coincidence problem for some specific scenarios known as the tracker models [7,8] in which the scalar field energy density tracks the background energy density in the past and takes over matter during the recent past. A power law potential can give rise to tracker solutions for larger negative values of the exponent [7,8]. But the problem with this scenario is that the EOS of the scalar field can be much greater than -1 at present for some potentials like power law potentials [8]. However, the advantage is that the late time solution is independent of a wide range of initial conditions, as it is an attractor solution which solves the coincidence problem. There is another class of scalar field models known as the thawing models [19,20]. In this scenario, the scalar field behaves as the CC in the past and starts evolving from the recent past which ensures the difference with the CC. Apart from these two dynamics, we can also have scaling behavior for steep exponential potential in which the scalar field scales the background energy density [21]. It is an attractor solution, so the scalar field scales forever in this dynamics. To exit from attractor scaling behavior, we need to modify the potential; e.g., the double exponential potential [22] or cosh potential [23] can give scaling behavior followed by late time acceleration. This dynamical behavior is generally known as the scaling-freezing dynamics.

Even though the CC is the most suitable explanation of late time acceleration, recent tensions in cosmology [24], e.g., tension in the measurements of the present value

[*]mhossain@jmi.ac.in
[†]afaq2206145@st.jmi.ac.in

of the Hubble parameter (H_0) [25,26] and the tension in the growth rate known as the $S_8 = \sigma_8\sqrt{\Omega_{\rm m0}/0.3}$ tension [24,27], where σ_8 is the standard deviation of matter density fluctuations at present for linear perturbation in spheres of radius $8h^{-1}$ Mpc, and $\Omega_{\rm m0}$ is the present value of the matter density parameter, raise the question about the validity of the standard Lambda cold dark matter (ΛCDM) model. The $\sim 5\sigma$ tension between the local measurement of H_0 by the SH0ES team ($H_0 = 73.04 \pm 1.04$ km sec^{-1} Mpc^{-1}) [25] and its constraint coming from the observation of the CMB radiation assuming the standard ΛCDM model ($H_0 = 67.4 \pm 0.5$ km sec^{-1} Mpc^{-1}) [3] has opened a new challenge in cosmology. The discrepancy between the two measurements can be due to systematic errors or some new physics is there [26,28–31]. To explain the tension with new physics, it is very clear that we have to go beyond ΛCDM. In this regard, scalar fields can play an interesting role as we can evade the tension, at least to some extent, by modifying the cosmic history either during early times or late times [26,30,32,33].

Modifying the early expansion of the Universe can be done by the early dark energy (EDE) scenario [14,15,34–36] where the scalar field density parameter (Ω_ϕ) has a small but finite value (< 0.1) during the matter radiation equality. Among the different EDE models [34], two scenarios have gained a lot of interest, one is the axionlike potential $\sim(1-\cos\phi)^n$ [12–15,34,35] and the another is the power law potential $\sim\phi^{2n}$ [16,36], where n is a constant. The axionlike potential has minima, and around the minima the potential behaves like ϕ^{2n}, i.e., the power law potential for positive values of n. So, the axionlike potential has power law behavior around the minima, which should give similar dynamics of the scalar field during the late time when the scalar field rolls near the minima for positive values of n. The possible deviation in oscillations in the two potentials have been studied in [37]. Now, the question remains whether the scalar field dynamics is different in the two potentials during the early times when the scalar field is away from the minima, and if it is, then is it significant? We address these issues in this paper. We also explore the dynamics for negative values of n. Even though the axionlike potential reduces to a power law potential around the minima for positive values of n, the dynamics of the scalar field can be different for negative values of n as the axionlike potential still has a minima but the power law is a runaway potential. This difference in the nature of the potentials can lead to distinguishable features in the cosmological dynamics, and therefore we examine this in detail. In this paper, our aim is to compare the cosmological dynamics in two widely considered potentials and try to see if there is any degeneracy in the dynamics. In this regard, we also want to explore the effects of the functional form and the values of the functions $\lambda = V_\phi(\phi)/V(\phi)$ and $\Gamma = V_{\phi\phi}(\phi)V(\phi)/V_\phi(\phi)^2$, where $V(\phi)$ is the potential, and the subscript ϕ denotes the derivative with respect to ϕ, on the scalar field dynamics. In other words, we want to see whether the dynamics of the scalar field in the cosmological background depends on the nature of the potential solely or if the values and forms of the functions λ and Γ mainly decide the dynamics irrespective of the explicit functional form of the potential. To study this, we consider two potentials, axionlike and power law, phenomenologically as examples. To compare the dynamics in the two potentials, we first study the fixed points and their stability which turns out to be similar and does not give us any distinguishable information, so we analyze each scenario numerically. We also compare the EDE solutions in both potentials, and we argue that the EDE solutions are almost identical and we do not expect anything distinguishable.

We introduce the scenario with the background cosmological equations in Sec. II. In Sec. III, we study the stability of the fixed points by analyzing the dynamical system. The comparison has been done numerically in Sec. IV in which we first study the nature of potentials in Sec. IV A. Then, we study the dynamics for positive values of n in Sec. IV B. The study of negative values of n is done in Sec. IV C. The comparison in the EDE scenario for both potentials is done in Sec. V. In Sec. VI, we study the observational constraints on the model parameters for the tracker models in the axionlike potential. We finally summarize and conclude in Sec. VII.

II. THE MODEL

We consider the following action of a minimally coupled canonical scalar field:

$$\mathcal{S} = \int {\rm d}^4x\sqrt{-{\rm g}}\left[\frac{M_{\rm Pl}^2}{2}R - \frac{1}{2}\partial_\mu\phi\partial^\mu\phi - V(\phi)\right] + \mathcal{S}_{\rm B}, \qquad (1)$$

where $M_{\rm Pl} = 1/\sqrt{8\pi G}$ is the reduced Planck mass, $V(\phi)$ is the potential of the field, and $\mathcal{S}_{\rm B} = \mathcal{S}_{\rm m} + \mathcal{S}_{\rm r}$ with $\mathcal{S}_{\rm m}$ and $\mathcal{S}_{\rm r}$ being the actions for matter and radiation, respectively.

Variation of the action (1) with respect to the metric $g_{\mu\nu}$ gives Einstein's field equation

$$M_{\rm Pl}^2 G_{\mu\nu} = T_{({\rm m})\mu\nu} + T_{({\rm r})\mu\nu} + T_{(\phi)\mu\nu}, \qquad (2)$$

where

$$T_{(\phi)\mu\nu} = \phi_{;\mu}\phi_{;\nu} - \frac{1}{2}{\rm g}_{\mu\nu}(\nabla\phi)^2 - {\rm g}_{\mu\nu}V(\phi) \qquad (3)$$

is the energy-momentum tensor of the scalar field. Variation with respect to the scalar field ϕ gives the equation of motion of the scalar field

$$\Box\phi - \frac{{\rm d}V}{{\rm d}\phi} = 0. \qquad (4)$$

In flat Friedmann-Lemaître-Robertson-Walker geometry with metric

$$ds^2 = -dt^2 + a(t)^2\delta_{ij}dx^i dx^j, \tag{5}$$

where $a(t)$ is the scale factor, the Friedman equations are given by

$$3H^2M_{\rm Pl}^2 = \rho_{\rm m} + \rho_{\rm r} + \frac{1}{2}\dot{\phi}^2 + V(\phi), \tag{6}$$

$$(2\dot{H} + 3H^2)M_{\rm Pl}^2 = -\frac{1}{3}\rho_{\rm r} - \frac{1}{2}\dot{\phi}^2 + V(\phi), \tag{7}$$

where $H = \dot{a}/a$ is the Hubble parameter with the dot representing the derivative with respect to time. $\rho_{\rm m}$ and $\rho_{\rm r}$ are the matter and radiation energy densities, respectively. The energy density and pressure of the scalar field are given by

$$\rho_\phi = \frac{1}{2}\dot{\phi}^2 + V(\phi), \tag{8}$$

$$p_\phi = \frac{1}{2}\dot{\phi}^2 - V(\phi). \tag{9}$$

The equation of motion of the scalar field has the standard form

$$\ddot{\phi} + 3H\dot{\phi} + \frac{{\rm d}V}{{\rm d}\phi} = 0. \tag{10}$$

In this paper, we are going to study the background cosmological dynamics of the scalar field for an axionlike potential given by [12,14,15,35]

$$V(\phi) = V_0\left(1 - \cos\left(\frac{\phi}{f_{\rm pl}}\right)\right)^n, \tag{11}$$

where V_0, $f_{\rm pl}$, and n are constants, and compare the same for the power law potential [16]

$$V(\phi) = V_0\left(\frac{\phi}{f_{\rm pl}}\right)^{2n}. \tag{12}$$

The axionlike potential (11) is periodic in nature, which repeats itself after one full cycle or time period. So, by any simple transformation in the scalar field, we can go from one cycle to any cycle that does not affect the dynamics of the scalar field. That means we can study the dynamics of the scalar field in one cycle as the dynamics will be the same in each full cycle. Also, as a periodic function, the axionlike potential has maxima and minima, and around the minima the axionlike potential reduces to the power law potential. In the following discussion of this paper, we compare the cosmological dynamics of the scalar field in these two potentials for both positive and negative values of the parameter n.

III. DYNAMICAL SYSTEM ANALYSIS

To compare the dynamics of the scalar field in the axionlike (11) and power law (12) potentials, we first study the dynamical system for the axionlike potential and analyze the nature of stability of the fixed points. This gives us the idea about the stability of the background cosmological solutions for the axionlike potential (for the power law potential, see Ref. [38]). So, in this section, we examine whether we get any specific fixed points which can distinguish the dynamics of the scalar field for the axionlike potential from the power law potential. To form the dynamical system, we define the following dimensionless variables:

$$x = \frac{\dot{\phi}}{\sqrt{6}H\,M_{\rm Pl}}, \tag{13}$$

$$y = \frac{\sqrt{V}}{\sqrt{3}H\,M_{\rm Pl}}, \tag{14}$$

$$\Omega_{\rm r} = \frac{\rho_r}{3H^2M_{\rm Pl}^2}, \tag{15}$$

$$\lambda = -M_{\rm Pl}\frac{V_\phi(\phi)}{V}, \tag{16}$$

$$\Gamma = \frac{V_{\phi\phi}(\phi)V(\phi)}{V_\phi(\phi)^2}. \tag{17}$$

While the variable λ signifies the slope of the potential, the variable Γ represents the nature of the potential; e.g., $\Gamma = 1$ for an exponential potential of constant slope λ. For the axionlike potential (11),

$$\lambda = -\frac{n}{f}\cot\left(\frac{\phi}{2f_{\rm pl}}\right), \tag{18}$$

$$\Gamma = 1 - \frac{1}{2n} - \frac{n}{2f^2\lambda^2}, \tag{19}$$

where $f = f_{\rm pl}/M_{\rm Pl}$. For the power law potential (12),

$$\lambda = -\frac{2n}{(\phi/M_{\rm Pl})}, \tag{20}$$

$$\Gamma = 1 - \frac{1}{2n}. \tag{21}$$

The function Γ represents the nature of the potential and from Eqs. (19) and (21) we can see that the difference in the functional form of Γ for the two potentials is the last term of Eq. (19). This term can be negligible for large values of the

slope λ which makes both Γ's identical. So, the scalar field dynamics is expected to be similar for both potentials, though it will also depend on the values of λ. Now, it would also be interesting to see whether the last term of Eq. (19) makes any significant difference in the dynamics of the scalar field. In this section, we look for these answers by doing fixed points analysis. In the next section, we discuss the effects of the nature and values of the functions λ and Γ on the dynamics of the scalar field for both potentials.

From Eq. (6), we see that the dimensionless variables follow the constraint equation $x^2+y^2+\Omega_{\rm r}+\Omega_{\rm m}=1$, where $\Omega_{\rm m}=\rho_m/3H^2M_{\rm Pl}^2$ is the density parameter of matter. The density parameter of the scalar field is defined as $\Omega_\phi=x^2+y^2$, while $\Omega_{\rm r}$ is that for radiation. The effective EOS and the EOS of the scalar field, in terms of the dimensionless variables, are given by

$$w_{\rm eff}=-\left(1+\frac{2}{3}\frac{\dot{H}}{H^2}\right)=x^2-y^2+\frac{1}{3}\Omega_{\rm r}, \tag{22}$$

$$w_\phi=\frac{\frac{1}{2}\dot{\phi}^2-V(\phi)}{\frac{1}{2}\dot{\phi}^2+V(\phi)}=\frac{x^2-y^2}{x^2+y^2}. \tag{23}$$

The evolution of the Universe is represented by Eqs. (7) and (10), which can be recast in terms of the evolution equations of the dimensionless variables (13)–(16) by the following autonomous system:

$$\frac{dx}{dN}=-\frac{3}{2}x\left(1-x^2+y^2-\frac{1}{3}\Omega_r\right)+\sqrt{\frac{3}{2}}y^2\lambda, \tag{24}$$

$$\frac{dy}{dN}=\frac{3}{2}y\left(1+x^2-y^2+\frac{1}{3}\Omega_r\right)-\sqrt{\frac{3}{2}}xy\lambda, \tag{25}$$

$$\frac{d\Omega_{\rm r}}{dN}=-\Omega_{\rm r}(1-3x^2+3y^2-\Omega_{\rm r}), \tag{26}$$

$$\frac{d\lambda}{dN}=\sqrt{6}x\lambda^2(1-\Gamma)=\sqrt{\frac{3}{2}}x\left(\frac{\lambda^2}{n}+\frac{n}{f^2}\right), \tag{27}$$

where $N=\ln a$. Here we should mention that the autonomous system (24)–(27) is valid for $n\neq 0$, as apparently it seems that Eq. (27) diverges as $n\to 0$. For $n=0$, the potential (11) reduces to a constant potential, i.e., $\lambda=0$. So, the autonomous system will not contain the λ variable for $n=0$.

As we have already constructed the autonomous system, we can calculate the fixed points by equating Eqs. (24)–(27) to zero. Before that, we should notice from Eq. (18) that $0\leq|\lambda|<\infty$, and for $\lambda\to\infty$ Eq. (27) diverges, so the autonomous system (24)–(27) can give us the fixed points as long as λ is either zero or finite. To avoid this divergence problem, we define a new variable corresponding to λ as [38,39]

$$\xi=\lambda/(1+\lambda) \tag{28}$$

and rewrite the autonomous system. We can see that $0\leq\xi\leq 1$ for $0\leq\lambda\leq\infty$; i.e., ξ remains finite even if $\lambda\to\infty$.

In terms of ξ, the last terms of Eqs. (24) and (25) will have the factor $\xi/(1-\xi)$ which blows up for $\xi\to 1$. To avoid this divergence in the autonomous system, we use the transformation $dN\to(1-\xi)dN$ [38] which does not change the dynamical behavior of the system as there will be an overall multiplication of the term $(1-\xi)$ in the autonomous system but makes the dynamical system consistent around $\xi=1$ [38]. So, the final dynamical system, consistent around $\xi=1$, becomes

$$\frac{dx}{dN}=-\frac{3}{2}x(1-\xi)\left(1-x^2+y^2-\frac{1}{3}\Omega_r\right)+\sqrt{\frac{3}{2}}y^2\xi, \tag{29}$$

$$\frac{dy}{dN}=\frac{3}{2}y(1-\xi)\left(1+x^2-y^2+\frac{1}{3}\Omega_r\right)-\sqrt{\frac{3}{2}}xy\xi, \tag{30}$$

$$\frac{d\Omega_{\rm r}}{dN}=-\Omega_{\rm r}(1-\xi)(1-3x^2+3y^2-\Omega_{\rm r}), \tag{31}$$

$$\frac{d\xi}{dN}=\sqrt{\frac{3}{2}}x(1-\xi)\left(\frac{\xi^2}{n}+\frac{n(1-\xi)^2}{f^2}\right). \tag{32}$$

The fixed points of the autonomous system (29)–(32) with their nature of stability are listed in the Table I. We can see that the fixed points and their stability are similar to the power law potential (12) [38]. The difference comes in the points $D_\pm$; as for the power law potential, these points are nonhyperbolic, but for the potential (11) we have hyperbolic points with the same condition on n for the nature of stability. From Table I, we can see that in the cosmological dynamics of an axionlike potential, we can have three stable points the same as the power law potential [38]. Point C is stable for n, $x>0$. We have shown this in Fig. 1 in the $y-\xi$ plane by considering fixed values of x and $\Omega_{\rm r}$. We can see that if we perturb the system from the fixed point (0,1) in the $y-\xi$ plane, then all trajectories move toward the fixed point C for n, $x>0$ which ensures the stable nature of point C. Similarly, in the upper panel of Fig. 2, we have shown the stable nature of the fixed points $D_\pm$ for $n=-2<0$ in the $x-\xi$ plane. In this panel, all the trajectories are moving toward the fixed points $D_\pm$. On the other hand, the lower panel of Fig. 2 shows that some of the trajectories are moving toward the fixed points $D_\pm$ and some of them are going away from it for $n=2>0$ in the $x-\xi$ plane. This shows the saddle nature of the fixed points $D_\pm$ for positive values of n.

From Table I, we can see from the fixed point analysis, only the $D_\pm$ points can give rise to late time acceleration with $w_{\rm eff}=w_\phi=-1$ and $\Omega_\phi=1$ only for $n<0$. For $n>0$, the only stable point is the point C, which cannot

TABLE I. Fixed points of the autonomous system (29)–(32) with their nature of stability and the values of different cosmological parameters at the fixed points are listed.

Point	x	y	Ω_r	ξ	Eigenvalues	Existence	Hyperbolicity	Stability	Ω_m	Ω_ϕ	w_ϕ	$w_{\rm eff}$
A	0	0	1	Any	$0, 2(1-\xi), 1-\xi, -(1-\xi)$	All n	Nonhyperbolic	Saddle for $\xi \neq 1$	0	0	Indeterminate	$1/3$
B	0	0	0	Any	$0, \frac{3}{2}(1-\xi), -(1-\xi), -\frac{3}{2}(1-\xi)$	All n	Nonhyperbolic	Saddle for $\xi \neq 1$	1	0	Indeterminate	0
C	x	0	Ω_r	1	$0, 0, -\frac{1}{n}\sqrt{\frac{3}{2}}x, -\sqrt{\frac{3}{2}}x$	Finite n	Nonhyperbolic	Stable for $n>0$ and $x>0$ (Fig. 1) Saddle for $x<0$ or $n<0$ and $x>0$ Unstable for $n>0$ and $x<0$	$1-x^2-\Omega_r$	x^2	1	$x^2+\frac{1}{3}\Omega_r$
$D_\pm$	0	± 1	0	0	$-4, -3, -\frac{3}{2}\left(1+\sqrt{1+\frac{2}{3}n}\right), -\frac{3}{2}\left(1-\sqrt{1+\frac{2}{3}n}\right)$	All n	Hyperbolic	Stable for $n<0$ Saddle for $n>0$ (Fig. 2)	0	1	-1	-1

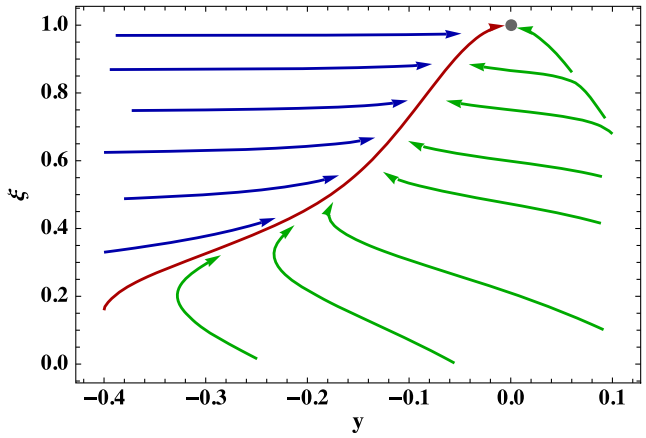

FIG. 1. Nature of stability of the point C for n, $x > 0$ in the $y-\xi$ plane. The gray dot represents the point C, i.e., $(y, \xi) \equiv (0, 1)$. We have considered $n = 2$, $x = 0.02$, and $\Omega_r = 0$.

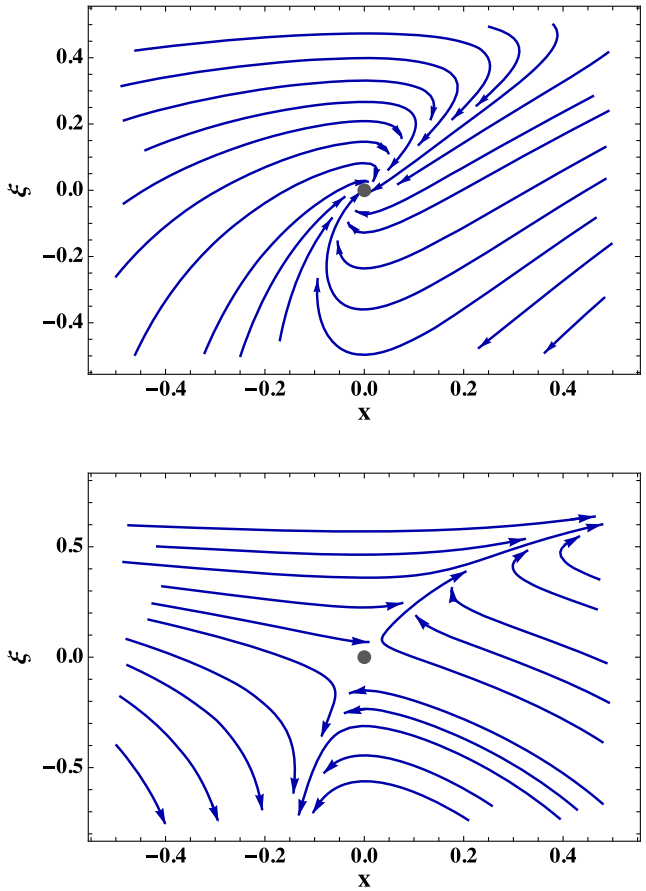

FIG. 2. The nature of stability of point D for $n = -2$ (upper panel) and $n = 2$ (lower panel) is shown in the $x-\xi$ plane. The gray dot represents the points $D_\pm$, i.e., $(x, \xi) \equiv (0, 0)$. We have considered $y = 1$. Here we have also shown the region $\xi > 1$ to show the nature of the trajectories properly.

give rise to late time acceleration. This point, in fact, cannot give any viable cosmological solution as it is an attractor solution also in the case of the power law potential [38], which means for $n > 0$, apparently, we do not have any late time acceleration solution. But that is not the case, as from the fixed point analysis we do not have the full dynamics of the system. This can be considered as a limitation of the dynamical system analysis. This will be clearer in the next section where we discuss the dynamics with the numerical results by analyzing the nature of the potentials as well as the corresponding functions of λ and Γ.

IV. NUMERICAL STUDY OF THE DYNAMICS

In this section, we discuss the dynamics of the scalar field qualitatively and point out the missing information about the dynamics in the fixed point analysis.

A. Nature of axionlike and power law potentials

In Fig. 3, we show the nature of the axionlike potential (11) and its corresponding slope λ (18) and $\Gamma - 1$ (19) for $n = 2$ (upper panel) and $n = -2$ (lower panel). Figure 4 shows the nature of the power law potential (12) and its slope λ for both positive and negative values of n. For the axionlike potential (Fig. 3), while the potential is continuous for positive values of n, it has periodic discontinuities for negative values of n. But within two discontinuities, the potential is continuous for negative values of n which can give us interesting cosmological solutions. Now, note that, for axionlike potential (11), the points of the maxima of the potential with positive values of n become the points of the minima for negative values of n, and the points of minima for the positive values of n become the points of discontinuity for the negative values of n. So, for both cases the potential has minima. Now, any minima at $\phi = \phi_0$ can be shifted to the origin by the transformation $\phi \to \phi \pm \phi_0$. For positive values of n, around the minima we can approximate the axionlike potential (11) as the power law potential (12). If we compare the upper panels of Figs. 3 and 4, we can see that in one cycle, around $\phi = 0$, the axionlike potential (11) has behavior similar to the power law potential (12) including the nature of their slopes. For $\phi > 0$, in the half cycle of axionlike potential (11), the slope varies from zero (at the maxima) to $-\infty$ (at $\phi = 0$), which is similar to the power potential for $\phi > 0$. The same similarity is there in the nature of the slopes for $\phi < 0$.

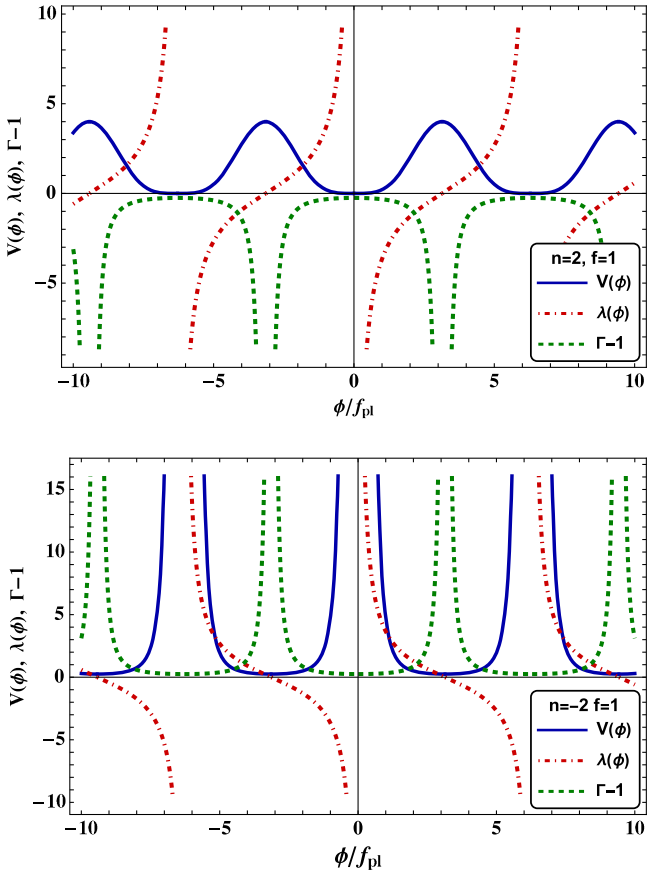

FIG. 3. Blue (solid), red (dot-dashed), and green (dashed) lines represent the potential (11) normalized by V_0, its slope (16), and corresponding $\Gamma - 1$ (19), respectively, for $n = 2$ (upper panel) and $n = -2$ (lower panel) with $f = 1$.

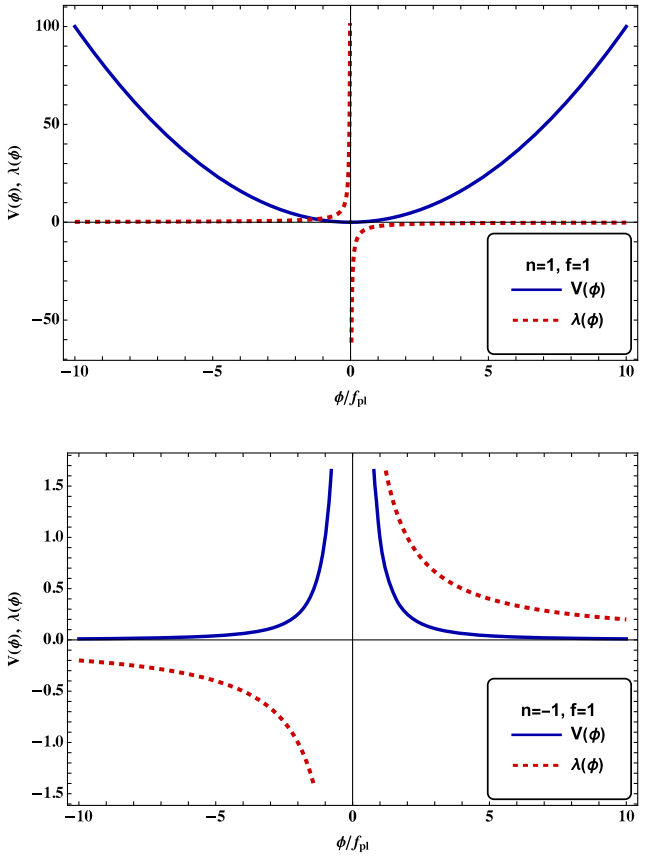

FIG. 4. Blue (solid) and red (dashed) lines represent the potential (12) normalized by V_0 and corresponding slope λ (20) for $n = 1$ (upper panel) and $n = -1$ (lower panel) with $f = 1$.

So, even though these two potentials apparently seem different, as the axionlike potential (11) is periodic in nature but the power law potential (12) is not, they have similarities in one cycle of the axionlike potential for positive values of n. These similarities in nature lead to the similarity in the cosmological dynamics of the scalar field in both potentials.

On the other hand, for negative values of n, the nature of the potentials and the corresponding functions of λ and Γ are different. From the lower panel of Fig. 3, we can see that the axionlike potential has minima, but from the lower panel of Fig. 4, we see that the power law potential is a runaway potential. These figures also show the difference in the slope of the potentials, but the important difference comes in the form of the function Γ as it becomes very large near the minima and becomes smaller as we go away from the minima for the axionlike potential (lower panel of Fig. 3), while it is a constant for the power law potential [Eq. (21)]. This is a major difference between the two potentials, and we shall see that this nature of the function Γ can lead to viable tracker solutions for the axionlike potential unlike the power law potential [7,8]. In this regard, the slope of the potential also has an important role to play, which we shall also discuss.

Apart from achieving the tracker solution, for negative values of n, another important thing to notice is that the minima of the axionlike potential (11), unlike the positive n case, is nonzero. This plays an important role in achieving CC-like behavior of the potential during the late time. The value of the potential at the minima would be $V_{\rm min} = 2^n V_0$. Now, to achieve CC-like behavior of the potential during late time, we can equate $V_{\rm min}^{1/4}$ with the dark energy scale $\rho_{\rm DE}^{1/4}$, where $\rho_{\rm DE}$ is the dark energy density which gives

$$V_0 \approx \frac{\rho_{\rm DE}}{2^n}, \quad \text{with} \quad n < 0. \tag{33}$$

From the above equation, we can see that once we fix the negative values of n, the scale of the axionlike potential (11) V_0 can be chosen suitably to achieve the proper dark energy scale. Here, we should mention that for the power law potential (12), with negative values of n, we cannot have CC-like behavior for physical values of ϕ. So, the existence of CC-like behavior in the axionlike potential (11) can make the potential (11) cosmologically viable along with tracker behavior.

B. Positive n and scaling solutions

In both potentials, for positive values of n, the scalar field will oscillate around the minima. During this oscillation, we can show that for a canonical scalar field $\langle \frac{1}{2}\dot{\phi}^2 \rangle = n\langle V(\phi)\rangle$, where the symbol $\langle \ldots \rangle$ represents the average value over one cycle [40,41]. So, the average EOS of the scalar field becomes

$$\langle w_\phi \rangle = \frac{n-1}{n+1}. \tag{34}$$

For $n = 1$, we have $\langle w_\phi \rangle = 0$, i.e., $\rho_\phi \sim a^{-3}$ like matter, while for $n = 2$, we have $\langle w_\phi \rangle = 1/3$ giving rise to $\rho_\phi \sim a^{-4}$ like radiation. When $n \ll 1$, we can have $\langle w_\phi \rangle \approx -1$, which may give rise to an accelerated phase of the Universe, so we can have different scalar field dynamics depending upon the values of n.

The function Γ, which tells us about the nature of the potential, plays an important role in determining the scalar field dynamics in the cosmological background. $\Gamma = 1$ for the exponential potential with constant slope, which gives rise to the scaling solution for $\lambda > \sqrt{3}$ [21]. For tracker dynamics, we need $\Gamma > 1$ [8]. From the upper panel of Fig. 3, we see that, for positive n, around the minima of the potential, $|\Gamma - 1|$ is also minimum, and as we increase the value of n it gets closer to zero around the minima which can be understood from Eq. (19). So, as we increase the value of positive n, there is a possibility of getting a scaling solution near the minima, as in this case Γ will be close to 1 and λ is very large, which means the potential can behave like a steep exponential one giving rise to scaling behavior. This same argument is also valid for the power law potential (12). From Eq. (21), we see that $\Gamma \approx 1$ for large positive values of n, and from the upper panel of Fig. 4, we see that the slope λ is large around the minima. So, also in the power law potential, we can get scaling solutions for larger positive values of n. In Fig. 5, we have shown the evolution of the scalar field energy density ρ_ϕ along with matter and radiation energy densities for $n = 3$ (dashed purple line) and $n = 20$ (solid blue line) for both potentials (upper panel for the axionlike potential and lower panel for the power law potential). We can see the similarity in the evolution of ρ_ϕ in both potentials for $n = 3$. This can easily be understood from Eq. (19), which tells us that when λ is very large, the function Γ becomes the same for both potentials. So, the axionlike potential basically reduces to a power law potential and gives rise to similar dynamics. We can also see that during the late times, ρ_ϕ decays faster than radiation, which follows Eq. (34).

We have already argued that larger positive values of n give rise to scaling solutions. Here, the solid blue line of Fig. 5, for $n = 20$, shows the scaling behavior of the scalar field dynamics for both potentials with the same initial conditions. In both panels, ρ_ϕ follows the matter during lower redshifts which gives $w_\phi \approx 0$. This behavior is an attractor solution. This tells us that the behavior of the scalar field dynamics during the lower redshifts is the same in both potentials, except that the power law potential reaches the attractor solution earlier than the axionlike potential for the same initial conditions. The reason behind this can be understood from Eqs. (19) and (21), which tell us that the difference between the function Γ of the two

potentials is the last term of Eq. (19). For finite values of n, this term is negligible only when $\lambda \to \infty$, as around the maxima of the axionlike potential, λ is very small and the last term of Eq. (19) remains non-negligible, which makes $\Gamma < 1$, i.e., away from behaving like an exponential potential, which means away from scaling solutions. So, if we fix the initial conditions around the maxima, which is the case for Fig. 5, the scalar field will take some time to reach the scaling solutions until the slope λ becomes sufficiently large. Until then, it will follow the dynamics which will be sensitive to the initial conditions. And, if we consider very large values of n, e.g., $n = 20$, before reaching the scaling solutions, $\rho_\phi \sim a^{-6}$ which makes ρ_ϕ much smaller than the background energy density. This causes large Hubble damping. Because of this damping, the scalar field freezes to evolve, causing it to behave like a CC. This CC-like behavior increases its energy density and it again starts evolving. Now, if λ is very large and $\Gamma \neq 1$, ρ_ϕ can repeat this behavior, and this is what is happening in the evolution of ρ_ϕ in the upper panel of Fig. 5 for $n = 20$ before reaching the attractor scaling solutions, i.e., at the higher redshifts. This difference in the dynamics at higher redshifts comes only for very large values of n. For $n = 3$, Fig. 5 shows that the dynamics is very similar in both the potentials. Also, we can reduce this difference even for large values of n by choosing suitable initial conditions. These similarities in the dynamics suggest to us that rather than the actual functional form of the potential, the form and the values of the functions λ and Γ determine the dynamics of the scalar field irrespective of the potential. So, there can be degeneracy in the dynamics of the scalar field for different potentials, as we have seen in this case.

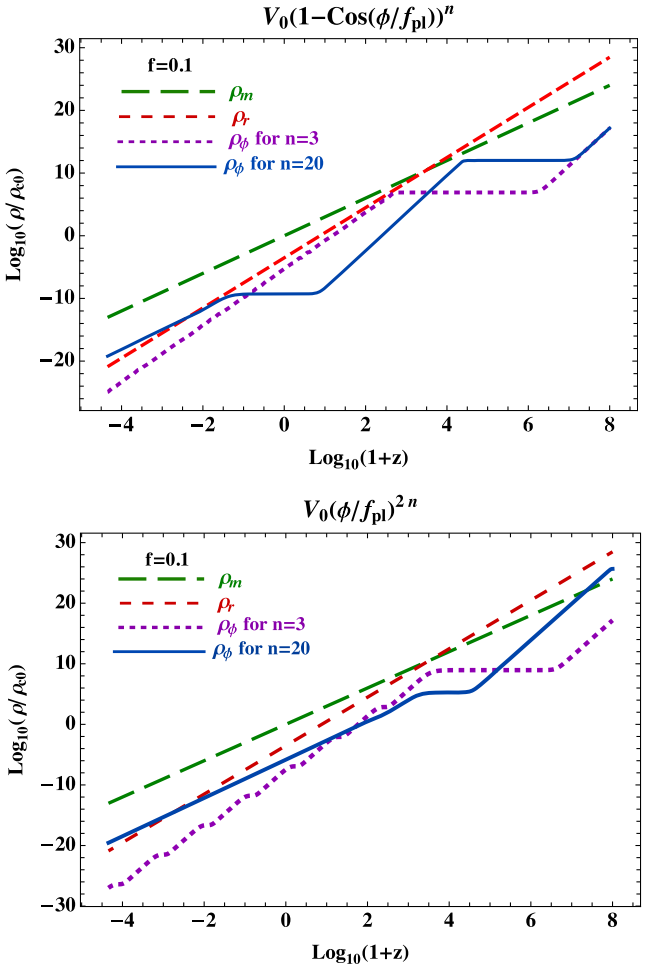

FIG. 5. Matter (long dashed green), radiation (short dashed red), and scalar field (solid blue for $n = 3$ and dashed purple for $n = 20$) energy densities normalized with the present value of critical density ρ_{c0} are shown for the axionlike potential (11) (upper panel) and power law potential (12) (lower panel). The same initial conditions have been considered by fixing the initial value of the field at $\phi_i/M_{\mathrm{Pl}} = \pi f - 0.004$ which is very close to the point of maxima for axionlike potential (11) and $\dot{\phi}_i/M_{\mathrm{Pl}} = 10^{-5}$ with $V_0 = 10^6\rho_{c0}$ and $f = 0.1$.

Here, we have another interesting thing to notice: Eq. (34) suggests that for large positive values of n, $w_\phi \to 1$. But, for $n = 20$, instead of having $w_\phi \approx 1$, we have $w_\phi \approx 0$, which does not follow Eq. (34). This suggests that for larger positive values of n, the oscillatory nature of the potentials may not be valid. In fact, numerically, we have seen that as we increase the positive values of n, the scalar field EOS follows Eq. (34) and increases toward 1 initially. But after some particular value of n, w_ϕ starts returning toward value $w_\phi = 0$. So, there is a turning point in w_ϕ, and we have seen that for $n > 3$, w_ϕ starts returning toward 0. In Fig. 6, we have shown the trajectories in the $\phi - \phi'$ plane, where the prime represents the derivative with respect to $\ln(1 + z)$ for increasing values of n from $n = 2$ to $n = 6$ for the axionlike potential. We can see that as we increase the values of n, the oscillations reduce and the oscillations cease to exist around $n > 5$. This clearly shows

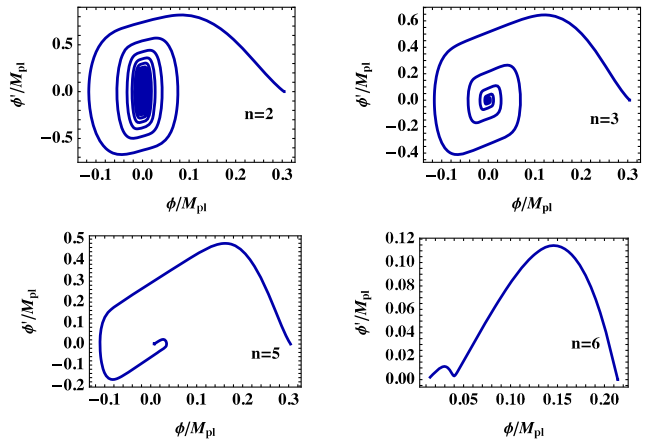

FIG. 6. Trajectories in the $\phi - \phi'$ plane are shown for the axionlike potential with $n = 2, 3, 5$, and 6. The same initial conditions $[\phi_i = (\pi f - 0.1)M_{\mathrm{Pl}}$ and $\phi' = 10^{-5}M_{\mathrm{Pl}}]$, $f = 0.1$, and $V_0 = 10^6\rho_{c0}$ have been considered for all panels.

that for larger values of n, the axionlike or power law potential becomes nonoscillatory. In Ref. [36] also, this nature of turnaround in w_ϕ has been shown for the power law potential, but this nature is also present in the axionlike potential. The physical reason behind this is that for larger positive values of n, the minima of both potentials become wider, which makes it less oscillatory.

C. Negative n and tracker solutions

While we get similar behavior in the cosmological dynamics of the scalar field in the axionlike (11) and power law (12) potentials for positive values of n, we shall see, as we discuss further, for negative values of n the dynamics is very distinguishable in terms of the tracker solutions and existence of CC-like behavior. In fact, the axionlike potential has the ability to make the tracker solutions more viable than the power law potential, as the axionlike potential (11) exhibits CC-like behavior during late time for negative values of n as discussed above by fixing the scale of the potential V_0 by the dark energy scale using Eq. (33). For negative values of n, from Eqs. (19) and (21), we can see that $\Gamma - 1$ will be symmetrically opposite to the one for positive n for both potentials. From the lower panel of Fig. 3 we can see that, for the axionlike potential, $\Gamma - 1$ is minimum near the point of discontinuity and becomes larger as we approach the minima of the potential where the slope λ is also very small. This nature in the functions λ and Γ can give rise to interesting dynamics of the scalar field. As the scalar field rolls down the potential from larger slope to much smaller slope, towards the minima, it can result to late time acceleration. At the same time, Γ increases and eventually it becomes > 1, which can give rise to tracker behavior [7,8]. Initially, while rolling down, the value of $\Gamma - 1$ is small, and if it is close to zero the potential will behave like an exponential potential with a large slope giving rise to scalinglike behavior. Toward the bottom of the potential, since $\Gamma - 1$ becomes large and λ becomes small the scalinglike behavior is followed by a slow roll of the scalar field which may result in late time acceleration. As $\Gamma - 1$ eventually increases, in this case, we cannot get a perfect scaling behavior, rather, we get tracker behavior in the scalar field dynamics where the scalar field almost scales the background in the past and eventually exits from the scalinglike nature and takes over matter in the recent past (upper panel of Fig. 7). Figures 7 and 8 show the evolution of the energy densities and scalar field EOS for the axionlike and power law potentials, respectively, for $n = -1$ and $n = -6$ with $f = 1$ and $\Omega_{\rm m0} \approx 0.3$. From both panels. we can see that the scalar field dynamics possesses the tracker behavior for $n = -6$.

For $n = -1$ we do not have tracker solutions, but the dynamics is more close to thawing dynamics [19,20], which gives rise to viable cosmology but can be very sensitive to initial conditions. From Fig. 7 we see that as

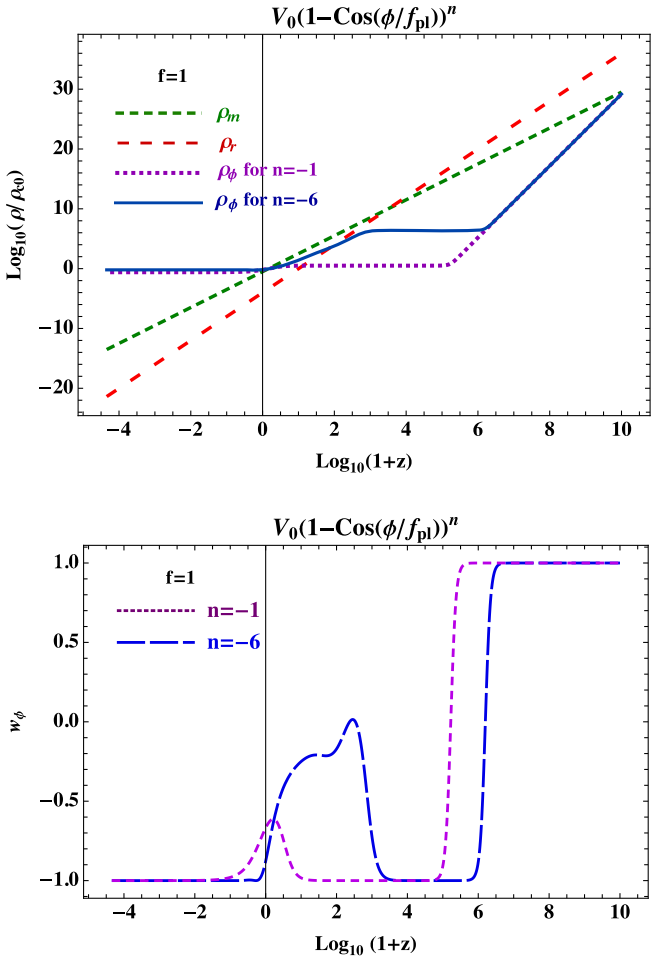

FIG. 7. Upper panel: matter (short dashed green), radiation (long dashed red), and scalar field (dotted purple for $n = -1$ and solid blue for $n = -6$) energy densities normalized with the present value of critical density ρ_{c0} are shown. Lower panel: scalar field EOS is shown for $n = -1$ (dotted purple) and $n = -6$ (dashed blue). Initial conditions are fixed by considering the present value of matter density $\Omega_{m0} \approx 0.3$ for $f = 1$. Both panels are for axionlike potential (11).

we increase the negative values of n the tracker dynamics becomes more prevalent, e.g., for $n = -6$, the same as the power law potential [7] (Fig. 8). But from the lower panel of Fig. 8, we see that for larger negative values of n, the present value of the scalar field EOS ($w_{\phi 0}$) becomes larger than -1, which can be disfavored by the data [3]. On the other hand, from the lower panel of Fig. 7, we can see that for the axionlike potential we get $w_{\phi 0} \approx -1$, even for larger negative values of n as λ becomes very small around the minima, and at some point it becomes close to zero, while for the power law potential, the slope becomes negligibly small only asymptotically. So, while for the power law potential the tracker solutions may not be viable for the axionlike potential, the scenario changes drastically, which has been depicted in Fig. 9. Figure 9 compares the tracker

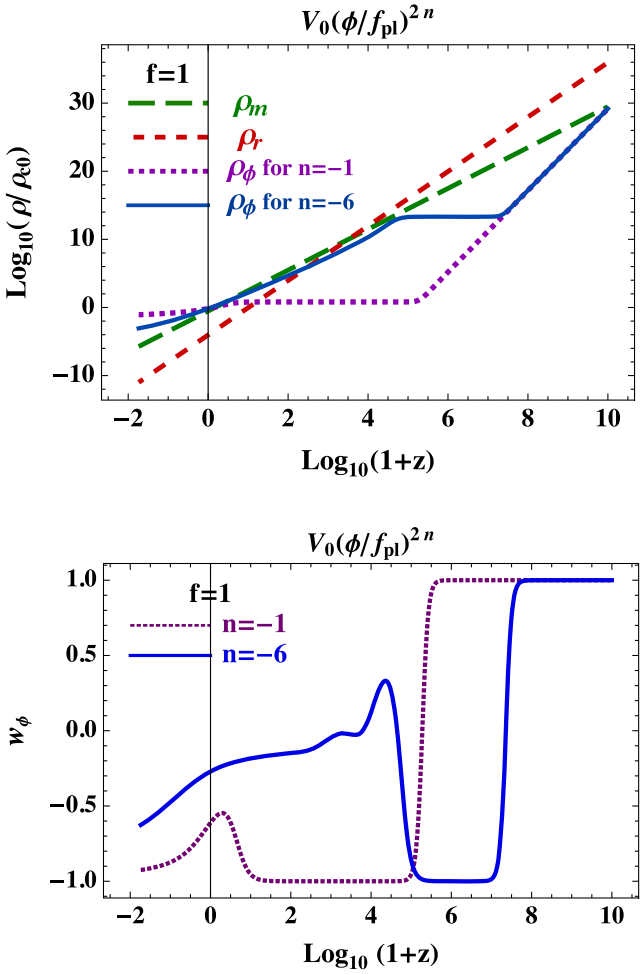

FIG. 8. Upper panel: matter (long dashed green), radiation (short dashed red), and scalar field (dotted purple for $n=-1$ and solid blue for $n=-6$) energy densities normalized with the present value of critical density ρ_{c0} are shown. Lower panel: scalar field EOS is shown for $n=-1$ (dotted purple) and $n=-6$ (solid blue). Initial conditions are fixed by considering the present value of matter density $\Omega_{m0}\approx 0.3$ and $f=1$, $V_0=1.6\rho_{c0}$, and $5\times 10^9\rho_{c0}$ for $n=-1$ and -6, respectively. Initial conditions are $\phi_i=0.5M_{\mathrm{Pl}}$ and $\phi_i'=10^{-3}M_{\mathrm{Pl}}$. Both panels are for power law potential (12).

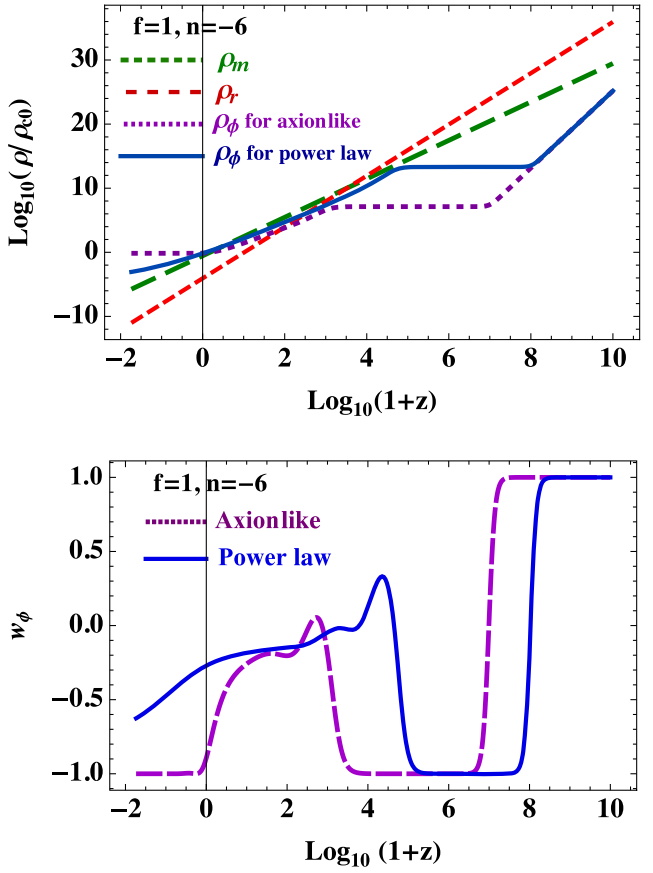

FIG. 9. Top panel: matter (short dashed green), radiation (long dashed red), and scalar field [dotted purple for axionlike potential (11) and solid blue for power law potential (12)] energy densities normalized with the present value of critical density ρ_{c0} are shown. Bottom panel: scalar field EOS is shown for axionlike potential (11) (dashed purple) and power law potential (12) (solid blue). Initial conditions are $\phi_i=0.5M_{\mathrm{Pl}}$ and $\phi_i'=10^{-5}M_{\mathrm{Pl}}$ for both potentials and fixed by considering the present value of matter density $\Omega_{m0}\approx 0.3$ with $f=1$ and $n=-6$, $V_0=44.79\rho_{c0}$ and $5\times 10^9\rho_{c0}$ for the axionlike and power law potentials, respectively.

solution in both potentials for $n=-6$ and $f=1$. The upper panel of Fig. 9 shows the evolution of the energy densities, which shows the tracker behavior of the scalar field in both potentials. The lower panel of Fig. 9 shows the evolution of the scalar field EOS in both potentials. It can easily be seen from the lower panel that the EOS of the scalar field is close the -1 at present for the axionlike potential, while it is away from -1 for the power law potential. If we increase the value of n, for the axionlike potential we can still get w_ϕ close to -1 at present, but for the power law potential the difference with -1 increases even further. The reason behind this is the existence of CC-like behavior in the axionlike potential (11) for negative values of n which can be achieved during the recent past depending upon the values of the parameter f. E.g., from the lower panel of Fig. 7, we can see that $w_\phi\approx -0.9$ at present and becomes -1 in the future for $f=1$ and $n=-6$. In this case, we reach the CC-like behavior in the future. But for lower values of f, this CC-like behavior can be reached in the recent past as depicted in Fig. 10. Figure 10 compares the tracker behavior in the axionlike and power law potentials for the same exponent with $f=0.3$ with the same initial conditions. From the lower panel of Fig. 10, we can see that the axionlike potential can have CC-like behavior from the recent past, which makes w_ϕ very close to -1, which cannot be achieved in the power law potential. In this regard, we should also note that the initial value of ϕ should be fixed away from the minima, as otherwise we cannot have any nontrivial or interesting dynamics. So, for negative values

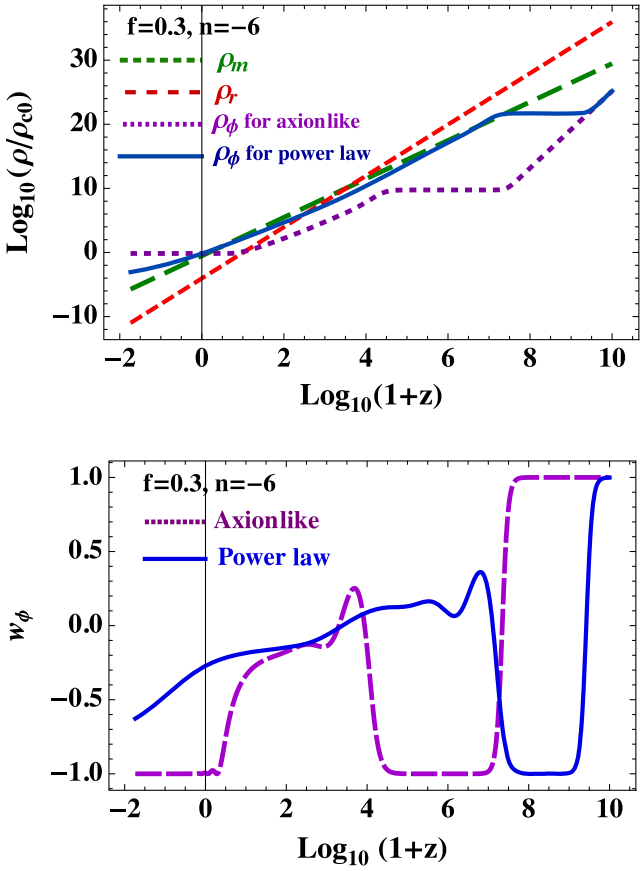

FIG. 10. Top panel: matter (short dashed green), radiation (long dashed red), and scalar field [dotted purple for axionlike potential (11) and solid blue for power law potential (12)] energy densities normalized with the present value of critical density ρ_{c0} are shown. Bottom panel: scalar field EOS is shown for axionlike potential (11) (dashed purple) and power law potential (12) (solid blue). Initial conditions are $\phi_i = 0.1M_{\rm Pl}$ and $\phi_i' = 10^{-5}M_{\rm Pl}$ for both potentials and fixed by considering the present value of matter density $\Omega_{m0} \approx 0.3$ with $f = 0.3$, $n = -6$ and $V_0 = 44.79\rho_{c0}$ and $10^{16}\rho_{c0}$ for the axionlike and power law potentials, respectively.

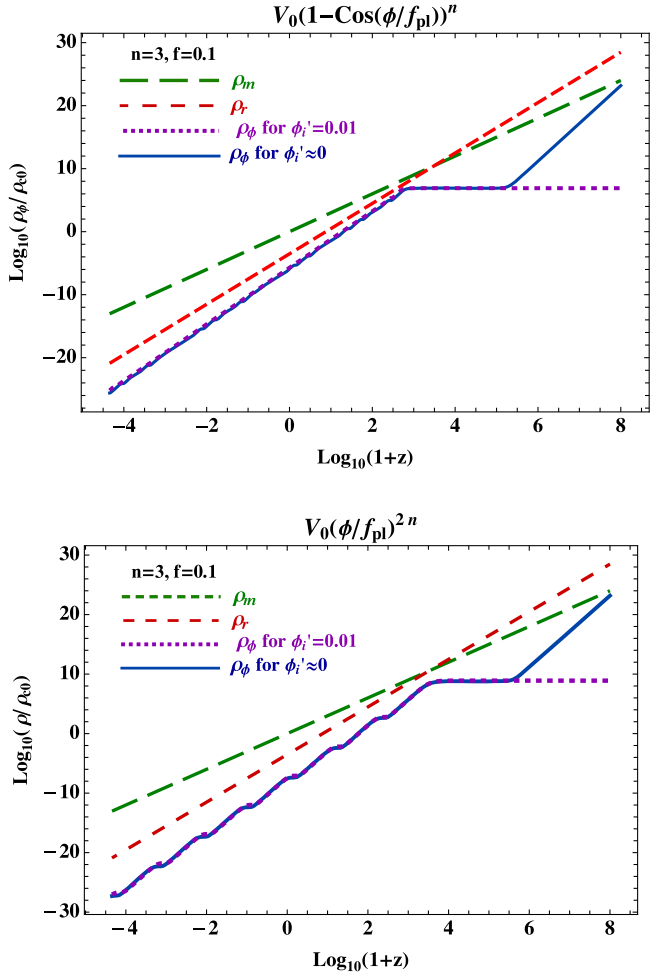

FIG. 11. Matter (long dashed green), radiation (short dashed red), and scalar field (solid blue for $\phi_i' = 0.01$ and dotted purple for $\phi_i' \approx 0$) energy densities normalized with the present value of critical density ρ_{c0} are shown for the axionlike potential (11) (upper panel) and power law potential (12) (lower panel). Both figures are for $\phi_i = \pi f - 0.01$, $n = 3$, $f = 0.1$, and $V_0 = 10^6\rho_{c0}$. In the figure, ϕ_i and ϕ_i' are normalized with $M_{\rm Pl}$.

of n, we have different behavior in the scalar field dynamics, which makes the two potentials distinguishable by making the tracker dynamics more cosmologically viable for the axionlike potential.

V. EARLY DARK ENERGY

EDE solutions can alleviate H_0 tension to some extent [14,15,34,36,42–48] by injecting a fraction of dark energy around the matter-radiation equality (MReq). This can be achieved with scalar fields if the scalar field freezes to evolve before the MReq, which leads to a CC-like behavior in the scalar field dynamics and increases the value of ρ_ϕ. Now, for viable cosmology, the scalar field cannot remain frozen, as this will result in cosmic acceleration much earlier. So, ρ_ϕ has to decay, and to avoid interfering with the structure formation, it has to decay fast around MReq which has been shown in Fig. 11. This nature in the scalar field dynamics can be seen in steep potentials [49] for which the scalar field eventually exhibits attractor scaling behavior as discussed above. In fact, the specific requirements in the EDE dynamics can be possible with scaling-freezing dynamics [50,51].

How EDE can be useful in alleviating the Hubble tension can be understood from the definition of the angle subtended by the comoving sound horizon r_s at the decoupling epoch $z_\star$ and it is given by

$$\theta_s = \frac{r_s(z_\star)}{D_A(z_\star)}. \tag{35}$$

θ_s is precisely measured by the CMB observations [3,5]. In the last equation, $D_A(z_\star)$ is the comoving angular diameter distance to the CMB surface of last scatter, and $r_s(z_\star)$ and $D_A(z_\star)$ are given by

$$r_s(z_\star) = \int_{z_\star}^{\infty} \frac{c_s(z)}{H(z)} dz = \frac{1}{H_\star} \int_{z_\star}^{\infty} \frac{c_s(z)}{H(z)/H_\star} dz, \quad (36)$$

$$D_A(z_\star) = c \int_0^{z_\star} \frac{dz}{H(z)} = \frac{c}{H_0} \int_0^{z_\star} \frac{dz}{E(z)}, \quad (37)$$

where $H_\star = H(z_\star)$, $E(z) = H(z)/H_0$, H_0 is the present value of the Hubble parameter, c is the velocity of light, and $c_s(z)$ is the sound speed of the photon-baryon fluid which is given by

$$c_s(z) = \frac{c}{\sqrt{3(1+R)}}, \quad (38)$$

$$R = \frac{3\omega_b}{4\omega_\gamma} \times \frac{1}{1+z}, \quad (39)$$

$$\omega_r = \left(1 + \frac{7}{8} N_{eff} \left(\frac{4}{11}\right)^{4/3}\right) \omega_\gamma, \quad (40)$$

where 100 km s^{-1} Mpc^{-1} $h = H_0$, $\Omega_{\gamma 0}$ is the photon density at present, $\omega_\gamma = \Omega_{\gamma 0} h^2 = 2.47 \times 10^{-5}$, Ω_{b0} is the baryon density at present, $\omega_b = \Omega_{b0} h^2 = 0.0224 \pm 0.0001$, $100\theta_s = 1.0411 \pm 0.0003$, and $N_{eff} = 3.06$ [3,25]. The limits of the integration of Eqs. (36) and (37) are very important, as one can understand that if we modify the cosmic history only around $z_\star$ and keep it the same as the standard model for $z < z_\star$, then the comoving sound horizon r_s will be changed. Now, the term within the integration in the definition of D_A will remain the same, as $E(z)$ does not change for $z < z_\star$. But, θ_s is precisely measured, which means it cannot be changed. This forces H_0 to change to keep θ_s fixed. So, by injecting EDE around $z_\star$, we can increase the expansion rate, which decreases the value of $r_s(z_\star)$, which forces H_0 to increase so that θ_s remains fixed.

The axionlike and power law potentials are two widely studied potentials as EDE solutions. EDE solutions can be achieved for the positive values of n in both potentials [14,15,35,36]. As we have already argued that for positive values of n the dynamics in both potentials is almost the same, we expect that the EDE solutions will also be the same in both potentials. In Fig. 11, the EDE solutions in both potentials have been shown for the same initial conditions and parameter values. We can see the similarity in the evolution of ρ_ϕ in both potentials except in the values of Ω_{EDE}, which is clear from the upper panel of Fig. 12 where the evolution of the EDE density parameter (Ω_{EDE}) in both scenarios has been shown. Note that, $\phi = \pi f$ is a maxima of the axionlike potential, and we have chosen the initial value of the field $\phi_i = \pi f - 0.01$, which is very close

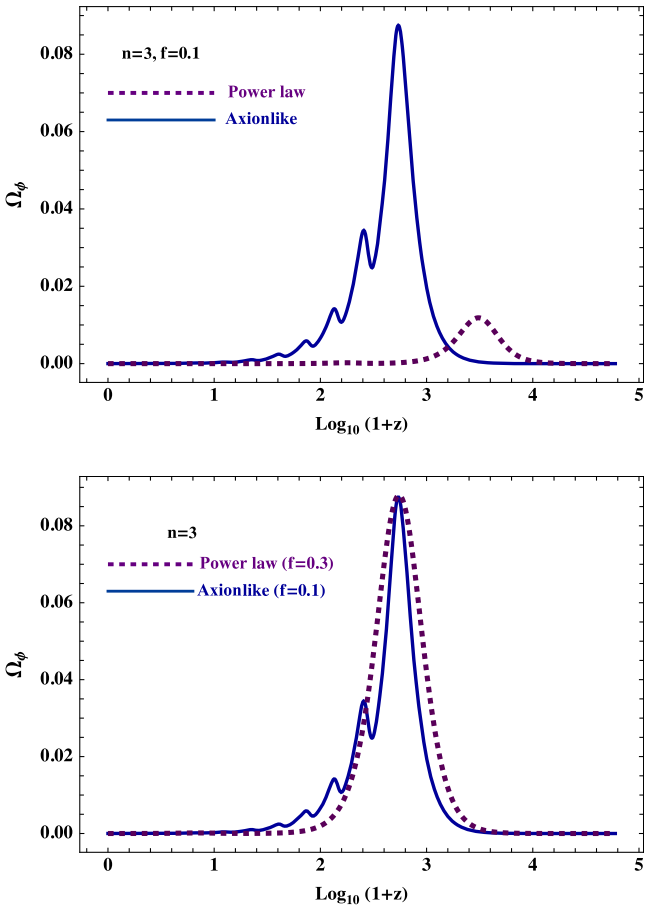

FIG. 12. Scalar field density parameter for the axionlike potential (solid blue) and power law potential (dashed purple) are shown. Upper panel is for the same initial values of $\phi_i = \pi f - 0.01$ and $\phi_i' \approx 0$ with $V_0 = 10^6 \rho_{c0}$. Lower panel is for $V_0 = 2.5 \times 10^4 \rho_{c0}$ and $f = 0.3$ with $\phi = \pi f - 0.01$ for the power law potential, while these values are the same as the upper panel for the axionlike potential.

to the maxima. So, this is nearly the maximum possible difference that we can have in the values of Ω_{EDE} for the same initial conditions and parameter values. The upper panel of Fig. 12 shows the evolution of Ω_{EDE} for the same initial conditions and parameters, and we can see that the maximum value of Ω_{EDE} is larger in the axionlike potential, which also shows the deviation of the axionlike potential from the power law behavior. But as we have already argued, we can tune the initial conditions and the parameters to achieve a similar behavior in the Ω_{EDE} in both potentials, which has been shown in the lower panel of Fig. 12. In this panel, the values of V_0 and f are different in the two potentials. While V_0 sets the energy scale, f sets the initial value of ϕ. So, by changing the value of V_0 we have achieved the EDE at the same energy scale, and by changing the value of f we change the maximum value of Ω_{EDE} as $\Omega_{EDE,max} \approx V(\phi_c)$ where ϕ_c is the field value when the field is frozen. So, in both potentials we not only have same amount of EDE but their evolution is also the

same. And even if it differs, then that difference will have an insignificant effect on the background cosmological evolution. In Ref. [35], the observational constraints in both potentials have been studied, and it was found that the constraints on the model parameters were very similar. For both potentials, $n = 3$ comes out to be the best fit value for the parameter n, and the value of H_0 is 71.49 for the axionlike potential and 71.82 for the power law potential. So, we can see the results are similar, which justifies our arguments.

VI. OBSERVATIONAL CONSTRAINTS ON THE TRACKER MODELS FOR THE AXIONLIKE POTENTIAL

As the negative values of n give interesting cosmological solutions for axionlike potential (11) in terms of the tracker behavior, it is worth obtaining the observational constraints on the model parameters. We call the model of the axionlike potential with negative n the "tracker axion." For the purpose of obtaining the observational constraints on the parameters, we use the following data:

(i) Cosmic chronometer: CC data of the Hubble parameter compiled by Gomez-Valent and Amendola [52].
(ii) SH0ES data: The measurement of H_0 by the SH0ES Collaboration [25].
(iii) Pantheon: The distance modulus measurement of type Ia supernovae compiled in the latest Pantheon sample in terms of $E(z)$ [52].
(iv) CMB: The CMB shift parameter (R), acoustic scale (l_A) measurements, and the baryon density (ω_b) from the compressed likelihood for Planck 2018 results [3] obtained by Chen *et al.* [53].
(v) Baryon acoustic oscillations (BAO): 6dF survey ($z = 0.106$) [54], SDSS-MGS survey ($z = 0.15$) [55], eBOSS quasar clustering ($z = 1.52$) [56], anisotropic BAO measurements by BOSSDR12 at $z = 0.38, 0.51, 0.61$ [57] have been considered along with the BAO measurement by BOSS-DR12 using Lyman-α samples at $z = 2.4$ [58].
(vi) MASERS: We have also considered angular diameter distances data measured using water megamasers under the Megamaser Cosmology Project at redshifts $z = 0.0116, 0.0340, 0.0277$ for Megamasers UGC 3789 [59,60], NGC 6264 [61], and NGC 5765b, respectively [62].

We perform a Markov chain Monte Carlo analysis using the abovementioned observational data to constrain the model parameters. To do this, we use the publicly available code EMCEE [63]. To analyze the results and plot the contours of the model parameters, we use the publicly available Python package GetDist [64]. Our model parameters are $\{\Omega_{m0}, r_d, h, \Omega_{b0}, \Omega_{r0}, f, n\}$, where the present Hubble parameter is given by $H_0 = 100\ \mathrm{km\,sec^{-1}\,Mpc^{-1}} \times h$, the parameters f and n are the parameters from the choice of the potential (11), while the sound horizon at the drag epoch r_d, baryon, and radiation energy densities at present Ω_{b0} and Ω_{r0} appear due to incorporation of the BAO and CMB data. We have considered flat priors for the parameters, and the priors are given in Table II.

TABLE II. Prior of the parameters.

Parameter	Prior
Ω_{m0}	[0.2, 0.5]
r_d/Mpc	[130, 160]
h	[0.5, 0.8]
Ω_{b0}	[0.001, 0.1]
$\Omega_{r0} \times 10^5$	[3, 10]
f	[0.01, 0.7]
n	$[-1, -15]$

The observational constraints on the parameters are given in Table III for the tracker-axion model. We have also included the corresponding constraints on the parameters (except f and n) in the ΛCDM model to compare with the tracker-axion model. The marginalized posterior distribution of the parameters for the tracker-axion model is shown in Fig. 13. From Table III, we see that the constraints on the parameters in both models are similar. This can be understood from Fig. 10. From Fig. 10, we see that the late time behavior of the axion field for negative values of n is very similar to the CC for lower values of the parameter f which has an upper bound $f < 0.11$ from the considered observational data (see Table III and Fig. 13). This nature of the EOS or energy density of the scalar field appears because the axionlike potential (11) with negative values of n has CC-like behavior around its minima, especially for $f < 1$, and the scalar field reaches near the minima of the potential during late time. In fact, we can relate the dark energy scale with the axionlike potential scale V_0 through Eq. (33). Also, unlike for the positive values of n, the axionlike potential (11) with negative values of n cannot give rise to sufficient EDE as it reaches tracker behavior and starts rolling a little before its energy density becomes sufficiently comparable to the background energy density to give rise to a finite amount of EDE. So, we do not expect any improvement in the present value of the Hubble parameter H_0. Also, because of the CC-like behavior of

TABLE III. Observational constraints of the parameters are given along with the corresponding constraints in the ΛCDM model.

Parameter	ΛCDM	Tracker axion
Ω_{m0}	0.299 ± 0.0067	$0.3004^{+0.0065}_{-0.0076}$
r_d/Mpc	144.6 ± 1.6	144.6 ± 1.6
h	0.699 ± 0.0063	0.6982 ± 0.0076
Ω_{b0}	0.046 ± 0.00083	$0.046^{+0.00092}_{-0.00074}$
$\Omega_{r0} \times 10^5$	4.914 ± 0.079	4.92 ± 0.1
f	⋯	<0.11
n	⋯	-7.8 ± 3.5

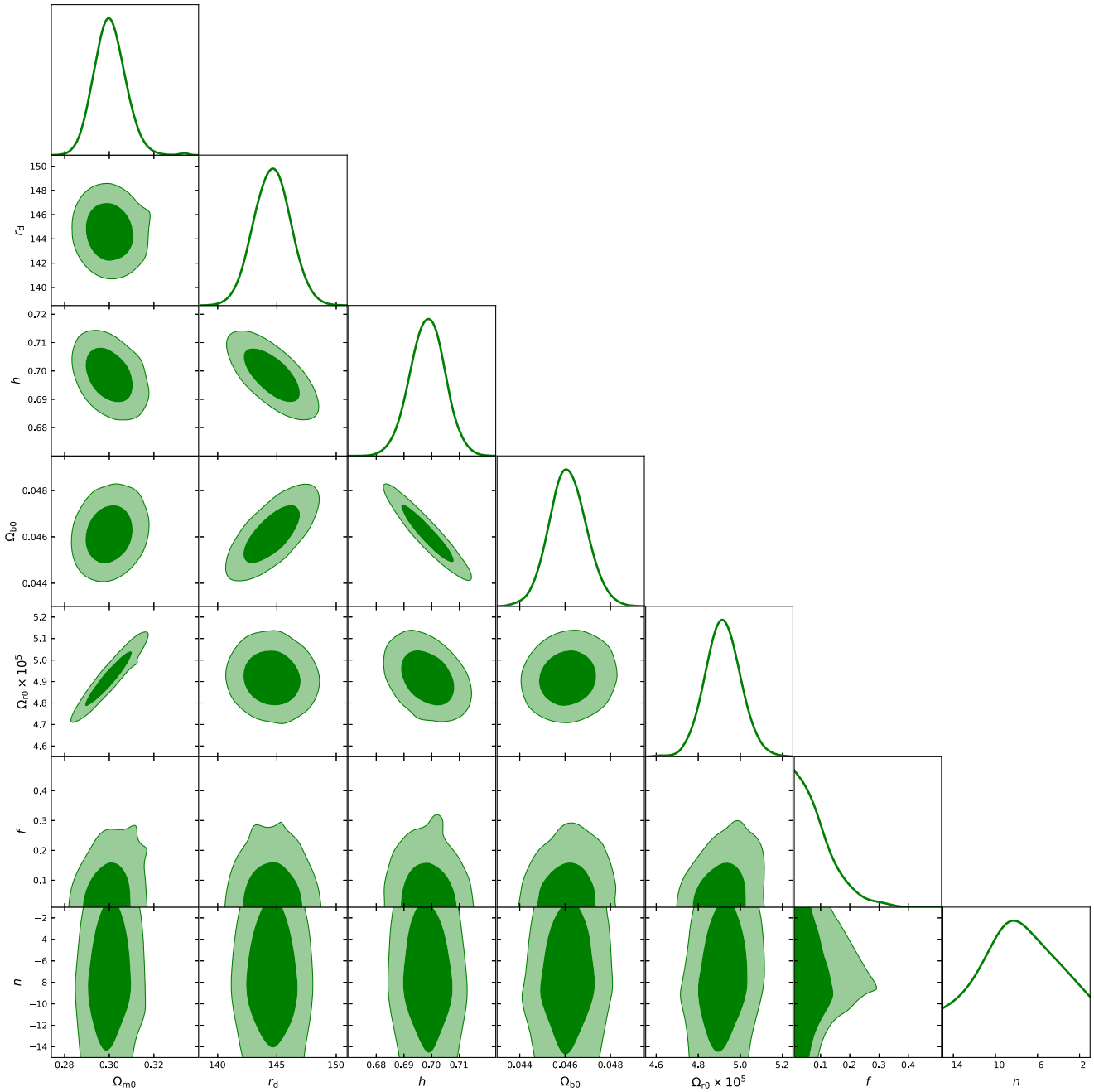

FIG. 13. Marginalized posterior distributions for the axionlike potential (11) with negative n. The data combination is CC + SH0ES + Pantheon + CMB + BAO + MASERS.

the axionlike potential with negative values of n around its minima, we expect that the constraint on the cosmological parameters would be similar to ΛCDM, which can be confirmed from Table III.

VII. DISCUSSION AND CONCLUSION

In this paper, scalar field dynamics in the cosmological background has been studied for axionlike (11) and power law (12) potentials. Both positive and negative values of the exponents have been considered. These potentials can give rise to EDE solutions and thus have the potential to reduce the H_0 tension [34]. We have studied the similarities between the two potentials in scalar field dynamics in a cosmological background. In this regard, first, we have studied the stability of the background cosmology using the fixed point analysis method. The fixed points and their stability are similar for both potentials except for the points $D_{\pm}$, which are hyperbolic points for the axionlike potential, unlike the power law potential for which these points are nonhyperbolic. So, the fixed point analysis has not given us

any new information about the dynamics of the scalar field and points toward the similarity between the axionlike and power law potentials. This motivates us to study the scenario for both potentials numerically.

We have then numerically studied the background cosmology for both potentials. Possible scaling and tracker solutions for both potentials have been explored. It has been found that for positive values of the exponent n, both potentials can exhibit scaling solutions for larger values of n and the dynamics is very similar. We do not have any distinguishable signature in any potential to differentiate. The reason behind this is that, for both potentials, for larger values of n, Γ approaches 1 while the slope λ approaches very large values (see Figs. 3 and 4). This scenario can be thought of as an exponential potential with large slope ($\lambda > \sqrt{3}$) which gives a scaling solution. Figure 5 shows the scaling behavior of the scalar field for the axionlike and power law potentials, respectively. We can see that, for the initial conditions they can reach the scaling regime at a different time. This can be understood from the expressions of Γ. From Eq. (21), we see that power law potential Γ is close to 1 for large values of n. So, the difference is in the last term of Eq. (19) which depends on λ. Now in Fig. 5, the scalar field's evolution is frozen twice, and it freezes for the first time at high redshifts for which n/λ^2 is finite. So, even for large values of n, Γ may not be close to 1 at high redshifts for axionlike potentials as the last term of Eq. (19) can still be finite. Therefore, it can repeat the dynamics for steep potentials [49] until λ becomes very large and $\Gamma \to 1$. But by tuning the initial conditions and choosing suitable parameter values, we can make λ large even at high redshifts, and the dynamics of the scalar field can be almost nondistinguishable in both potentials. So as long as the background cosmological dynamics is concerned, we can say that the axionlike and power law potentials can give rise to similar dynamics of the scalar field for positive values of n. In this regard, we should also mention that the two potentials have been studied as EDE solutions [14,15,36], and we expect the solutions to be almost degenerate which can also be seen in Ref. [35] where the authors have studied the oscillatory potentials, and the results for the axionlike and power law potentials are very similar.

Unlike the positive values of the exponent n, for negative values of n the background solutions are very distinct. In this scenario, both potentials can give rise to tracker solutions (see Figs. 7 and 8). For the power law potential, in tracker dynamics, the background cosmology may not be viable as the EOS of the scalar field, at present, becomes much larger than -1 (lower panel of Fig. 8). But, interestingly, for the axionlike potential the scenario changes drastically as we get viable cosmology with a tracker solution where the EOS of the scalar field is close to -1 at present (lower panels of Figs. 7, 9, and 10). This is a distinguishable feature of the axionlike potential for negative values of n. This discrepancy in the cosmological dynamics in the two potentials arises because of the nature of the Γ function. From Eqs. (19) and (21), we can see that the difference in these equations is in the last term of Eq. (19), which plays a crucial role for negative values of n but remains almost insignificant for positive values of n. As we can see from the lower panel of Fig. 3, Γ becomes much larger than 1 at the bottom of the potential where the slope λ becomes very small, giving rise to viable tracker solutions for the axionlike potential. In fact, this small value of λ leads to a CC-like behavior in the axionlike potential for negative n around the minima. Because of this CC-like behavior, we can relate the dark energy scale with the potential scale V_0 using Eq. (33). Also, due to this CC-like behavior, the observational constraint on the parameters is very similar to the constraint on the parameters for the ΛCDM model for the same set of cosmological data. This can be seen from Table III and Fig. 13. But for the power law potential, Γ remains constant and can be close to 1 for larger values of n [Eq. (21)], while its slope λ (20) becomes close to zero only asymptotically. In summary, we can conclude that considering the background cosmological dynamics of the scalar field, for positive n, we have degeneracy among the axionlike (11) and power law (12) potentials, but the degeneracy is broken for negative values of n for which we get viable tracker dynamics for the axionlike potential.

ACKNOWLEDGMENTS

The authors gratefully acknowledge the discussions regarding observational data analysis with Shahnawaz A. Adil, Sonej Alam, and Sumit Kumar. M. W. H. acknowledges the financial support from SERB, Government of India under the Start-up Research Grant No. SRG/2022/002234.

[1] A. G. Riess *et al.* (Supernova Search Team), Astron. J. **116**, 1009 (1998).
[2] S. Perlmutter *et al.* (Supernova Cosmology Project Collaboration), Astrophys. J. **517**, 565 (1999).
[3] N. Aghanim *et al.* (Planck Collaboration), Astron. Astrophys. **641**, A6 (2020); **652**, C4(E) (2021).
[4] D. Brout *et al.*, Astrophys. J. **938**, 110 (2022).
[5] P. A. R. Ade *et al.* (Planck Collaboration), Astron. Astrophys. **571**, A16 (2014).
[6] J. Martin, C. R. Phys. **13**, 566 (2012).
[7] I. Zlatev, L.-M. Wang, and P. J. Steinhardt, Phys. Rev. Lett. **82**, 896 (1999).

[8] P. J. Steinhardt, L.-M. Wang, and I. Zlatev, Phys. Rev. D **59**, 123504 (1999).
[9] E. J. Copeland, M. Sami, and S. Tsujikawa, Int. J. Mod. Phys. D **15**, 1753 (2006).
[10] V. Sahni and A. A. Starobinsky, Int. J. Mod. Phys. D **09**, 373 (2000).
[11] T. Clifton, P. G. Ferreira, A. Padilla, and C. Skordis, Phys. Rep. **513**, 1 (2012).
[12] D. J. E. Marsh, Phys. Rep. **643**, 1 (2016).
[13] R. Hlozek, D. Grin, D. J. E. Marsh, and P. G. Ferreira, Phys. Rev. D **91**, 103512 (2015).
[14] V. Poulin, T. L. Smith, T. Karwal, and M. Kamionkowski, Phys. Rev. Lett. **122**, 221301 (2019).
[15] V. Poulin, T. L. Smith, D. Grin, T. Karwal, and M. Kamionkowski, Phys. Rev. D **98**, 083525 (2018).
[16] B. Ratra and P. J. E. Peebles, Phys. Rev. D **37**, 3406 (1988).
[17] C. Wetterich, Nucl. Phys. **B302**, 645 (1988).
[18] C. Wetterich, Nucl. Phys. **B302**, 668 (1988).
[19] R. R. Caldwell and E. V. Linder, Phys. Rev. Lett. **95**, 141301 (2005).
[20] R. J. Scherrer and A. A. Sen, Phys. Rev. D **77**, 083515 (2008).
[21] E. J. Copeland, A. R. Liddle, and D. Wands, Phys. Rev. D **57**, 4686 (1998).
[22] T. Barreiro, E. J. Copeland, and N. J. Nunes, Phys. Rev. D **61**, 127301 (2000).
[23] V. Sahni and L.-M. Wang, Phys. Rev. D **62**, 103517 (2000).
[24] L. Perivolaropoulos and F. Skara, New Astron. Rev. **95**, 101659 (2022).
[25] A. G. Riess *et al.*, Astrophys. J. Lett. **934**, L7 (2022).
[26] M. Kamionkowski and A. G. Riess, Annu. Rev. Nucl. Part. Sci. **73**, 153 (2023).
[27] T. M. C. Abbott *et al.* (Kilo-Degree Survey and Dark Energy Survey Collaborations), Open J. Astrophys. **6** (2023), 10.21105/astro.2305.17173.
[28] W. L. Freedman and B. F. Madore, J. Cosmol. Astropart. Phys. 11 (2023) 050.
[29] J. L. Bernal, L. Verde, and A. G. Riess, J. Cosmol. Astropart. Phys. 10 (2016) 019.
[30] L. Knox and M. Millea, Phys. Rev. D **101**, 043533 (2020).
[31] L. Verde, N. Schöneberg, and H. Gil-Marín, arXiv:2311.13305.
[32] E. Di Valentino, O. Mena, S. Pan, L. Visinelli, W. Yang, A. Melchiorri, D. F. Mota, A. G. Riess, and J. Silk, Classical Quantum Gravity **38**, 153001 (2021).
[33] J.-P. Hu and F.-Y. Wang, Universe **9**, 94 (2023).
[34] V. Poulin, T. L. Smith, and T. Karwal, Phys. Dark Universe **42**, 101348 (2023).
[35] T. L. Smith, V. Poulin, and M. A. Amin, Phys. Rev. D **101**, 063523 (2020).
[36] P. Agrawal, F.-Y. Cyr-Racine, D. Pinner, and L. Randall, Phys. Dark Universe **42**, 101347 (2023).
[37] C. E. Norton and R. J. Scherrer, Phys. Rev. D **103**, 023515 (2021).
[38] S. Bahamonde, C. G. Böhmer, S. Carloni, E. J. Copeland, W. Fang, and N. Tamanini, Phys. Rep. **775–777**, 1 (2018).
[39] S. C. C. Ng, N. J. Nunes, and F. Rosati, Phys. Rev. D **64**, 083510 (2001).
[40] M. S. Turner, Phys. Rev. D **28**, 1243 (1983).
[41] M. C. Johnson and M. Kamionkowski, Phys. Rev. D **78**, 063010 (2008).
[42] T. Kodama, T. Shinohara, and T. Takahashi, Phys. Rev. D **109**, 063518 (2024).
[43] M.-X. Lin, G. Benevento, W. Hu, and M. Raveri, Phys. Rev. D **100**, 063542 (2019).
[44] F. Niedermann and M. S. Sloth, Phys. Rev. D **103**, L041303 (2021).
[45] F. Niedermann and M. S. Sloth, Phys. Rev. D **102**, 063527 (2020).
[46] K. V. Berghaus and T. Karwal, Phys. Rev. D **101**, 083537 (2020).
[47] K. V. Berghaus and T. Karwal, Phys. Rev. D **107**, 103515 (2023).
[48] T. Karwal, M. Raveri, B. Jain, J. Khoury, and M. Trodden, Phys. Rev. D **105**, 063535 (2022).
[49] C.-Q. Geng, M. W. Hossain, R. Myrzakulov, M. Sami, and E. N. Saridakis, Phys. Rev. D **92**, 023522 (2015).
[50] O. F. Ramadan, T. Karwal, and J. Sakstein, Phys. Rev. D **109**, 063525 (2024).
[51] E. J. Copeland, A. Moss, S. Sevillano Muñoz, and J. M. M. White, arXiv:2309.15295.
[52] A. Gómez-Valent and L. Amendola, J. Cosmol. Astropart. Phys. 04 (2018) 051.
[53] L. Chen, Q.-G. Huang, and K. Wang, J. Cosmol. Astropart. Phys. 02 (2019) 028.
[54] F. Beutler, C. Blake, M. Colless, D. H. Jones, L. Staveley-Smith, L. Campbell, Q. Parker, W. Saunders, and F. Watson, Mon. Not. R. Astron. Soc. **416**, 3017 (2011).
[55] A. J. Ross, L. Samushia, C. Howlett, W. J. Percival, A. Burden, and M. Manera, Mon. Not. R. Astron. Soc. **449**, 835 (2015).
[56] M. Ata *et al.* (eBOSS Collaboration), Mon. Not. R. Astron. Soc. **473**, 4773 (2018).
[57] S. Alam *et al.* (BOSS Collaboration), Mon. Not. R. Astron. Soc. **470**, 2617 (2017).
[58] H. du Mas des Bourboux *et al.* (BOSS Collaboration), Astron. Astrophys. **608**, A130 (2017).
[59] M. J. Reid, J. A. Braatz, J. J. Condon, L. J. Greenhill, C. Henkel, and K. Y. Lo, Astrophys. J. **695**, 287 (2009).
[60] M. J. Reid, J. A. Braatz, J. J. Condon, K. Y. Lo, C. Y. Kuo, C. M. V. Impellizzeri, and C. Henkel, Astrophys. J. **767**, 154 (2013).
[61] C. Kuo, J. A. Braatz, M. J. Reid, F. K. Y. Lo, J. J. Condon, C. M. V. Impellizzeri, and C. Henkel, Astrophys. J. **767**, 155 (2013).
[62] F. Gao, J. A. Braatz, M. J. Reid, K. Y. Lo, J. J. Condon, C. Henkel, C. Y. Kuo, C. M. V. Impellizzeri, D. W. Pesce, and W. Zhao, Astrophys. J. **817**, 128 (2016).
[63] D. Foreman-Mackey, D. W. Hogg, D. Lang, and J. Goodman, Publ. Astron. Soc. Pac. **125**, 306 (2013).
[64] A. Lewis, arXiv:1910.13970.